Citation: Cell Death and Disease (2012) 3, e280; doi:10.1038/cddis.2012.17

www.nature.com/cddis

C16 ceramide is crucial for triacylglycerol-induced apoptosis in macrophages

E Aflaki[1,2], P Doddapattar[1], B Radović[1], S Povoden[1], D Kolb[3,4], N Vujić[1], M Wegscheider[1], H Koefeler[3], T Hornemann[5], WF Graier[1], R Malli[1], F Madeo[6] and D Kratky*[,1]

Triacylglycerol (TG) accumulation caused by adipose triglyceride lipase (ATGL) deficiency or very low-density lipoprotein (VLDL) loading of wild-type (Wt) macrophages results in mitochondrial-mediated apoptosis. This phenotype is correlated to depletion of Ca^{2+} from the endoplasmic reticulum (ER), an event known to induce the unfolded protein response (UPR). Here, we show that ER stress in TG-rich macrophages activates the UPR, resulting in increased abundance of the chaperone GRP78/BiP, the induction of pancreatic ER kinase-like ER kinase, phosphorylation and activation of eukaryotic translation initiation factor 2A, the translocation of activating transcription factor (ATF)4 and ATF6 to the nucleus and the induction of the cell death executor CCAAT/enhancer-binding protein homologous protein. C16:0 ceramide concentrations were increased in *Atgl–/–* and VLDL-loaded Wt macrophages. Overexpression of ceramide synthases was sufficient to induce mitochondrial apoptosis in Wt macrophages. In accordance, inhibition of ceramide synthases in *Atgl–/–* macrophages by fumonisin B1 (FB1) resulted in specific inhibition of C16:0 ceramide, whereas intracellular TG concentrations remained high. Although the UPR was still activated in *Atgl–/–* macrophages, FB1 treatment rescued *Atgl–/–* macrophages from mitochondrial dysfunction and programmed cell death. We conclude that C16:0 ceramide elicits apoptosis in *Atgl–/–* macrophages by activation of the mitochondrial apoptosis pathway.
Cell Death and Disease (2012) **3,** e280; doi:10.1038/cddis.2012.17; published online 15 March 2012
Subject Category: Internal Medicine

Ceramides are bioactive sphingolipids that mediate anti-proliferative and pro-apoptotic signaling in response to various stress stimuli.[1] Ceramides serve as precursors for the biosynthesis of glycosphingolipids and sphingomyelin in the Golgi.[2,3] Ceramides are synthesized primarily by three pathways: (i) the *de novo* synthesis pathway from serine and palmitoyl-CoA catalyzed by serine palmitoyltransferase, (ii) the *salvage* pathway using ceramide synthases to produce ceramide from sphingosine and (iii) by sphingomyelinases, which hydrolyze sphingomyelin to produce ceramide. Mammalian (dihydro)ceramide synthases (CerSs) 1–6 have been identified as yeast homologues of the longevity assurance genes (Lass).[4,5] Each of the CerS family members regulates the synthesis of a specific subset of ceramides with different fatty acid chain-lengths and different saturation of fatty acyl-CoAs.[6] In neutrophils, *de novo*-generated C16- and C24-ceramides contribute to apoptosis.[7] The question which CerS and which ceramide species might be involved in macrophage apoptosis has not been addressed so far.

The endoplasmic reticulum (ER) is a critical organelle in the induction of apoptosis and is responsible for intracellular Ca^{2+} storage. The ER provides a membranous network for protein modifications and proper protein folding and assembly. Therefore, failure of this machinery to fold newly synthesized proteins or perturbations of the ER Ca^{2+} equilibrium present unique danger to the cell, which disrupt normal cellular functions termed as ER stress.[8,9] To combat the deleterious effects of ER stress, cells have evolved protective strategies named the unfolded protein response (UPR). This concerted and complex cellular response is mediated through three ER transmembrane receptors: protein kinase-like ER kinase (PERK), inositol-requiring enzyme 1 (IRE1) and activating transcription factor 6 (ATF6).[10–12] In resting cells, all three stress receptors are associated with the ER chaperone GRP78/BiP, which maintains the receptors in an inactive state.[8] On accumulation of unfolded proteins, GRP78 dissociates from the receptors, which leads to their activation and triggers the UPR.[8,9] During ER stress, all three

[1]Institute of Molecular Biology and Biochemistry, Center of Molecular Medicine, Medical University of Graz, Harrachgasse 21, 8010 Graz, Austria; [2]National Human Genome Research Institute/NIH Molecular Neurogenetics Section, 35 Convent Drive, Bethesda, MD, USA; [3]Institute of Cell Biology, Histology and Embryology, Medical University of Graz, Harrachgasse 21, 8010 Graz, Austria; [4]Center for Medical Research, Medical University of Graz, Stiftingtalstrasse 24, 8010 Graz, Austria; [5]Institute of Clinical Chemistry, University of Zurich, Rämistrasse 100, 8091 Zürich, Switzerland and [6]Institute of Molecular Biosciences, University of Graz, Humboldtstrasse 50, 8010 Graz, Austria
*Corresponding author: D Kratky, Institute of Molecular Biology and Biochemistry, Center of Molecular Medicine, Medical University of Graz, Harrachgasse 21, 8010 Graz, Austria. Tel: +43 316 380 7543; Fax: +43 316 380 9615; E-mail: dagmar.kratky@medunigraz.at
Keywords: adipose triglyceride lipase deficiency; triacylglycerol; C16 ceramide; lipotoxicity; macrophages; apoptosis
Abbreviations: ATF, activating transcription factor; Atgl, adipose triglyceride lipase; Asah1, acid ceramidase; Asah2, neutral ceramidase; BHQ, 2,5-di-*t*-butyl-1, 4-benzohydroquinone; CerS, (dihydro)ceramide synthase; CHOP, CCAAT/enhancer-binding protein homologous protein; complex 1, NADH/ubiquinone oxidoreductase; eIF2α, eukaryotic translation initiation factor 2A; ER, endoplasmic reticulum; FB1, fumonisin B1; IRE1, inositol-requiring enzyme 1; LPDS, lipoprotein-deficient serum; M-CSF, macrophage colony-stimulating factor; Noxa1, NADPH oxidase activator; p, phosphorylated; PERK, protein kinase-like ER kinase; PI, propidium iodide; ROS, reactive oxygen species; SERCA, sarcoplasmic/endoplasmic reticulum Ca^{2+} ATPase; TG, triacylglycerol; UPR, unfolded protein response; VLDL, very low-density lipoprotein; Wt, wild-type; XBP1, X-box-binding protein 1
Received 16.1.12; revised 02.2.12; accepted 07.2.12; Edited by RA Knight

arms of the UPR induce transcription of the cell death executor CCAAT/enhancer-binding protein homologous protein (CHOP/GADD153). For the upregulation of CHOP protein expression, the PERK-ATF6 branch of the UPR is essential.[8] IRE1 removes a 26-nucleotide intron from the X-box-binding protein 1 (XBP1) mRNA, previously induced by ATF6. The generated spliced XBP1 (sXBP1) encodes an active transcription factor. If the UPR has been successful, the ER returns to normal function and the cell survives.[8] In general, the UPR is a pro-survival response for reducing the accumulation of unfolded proteins and restore normal ER function.[13] However, if protein aggregation is persistent without eliminating the stress, signaling switches from pro-survival to pro-apoptotic pathways.

In macrophages, free cholesterol was shown to be a potent inducer of apoptosis.[14,15] Free cholesterol accumulation leads to caspase-dependent externalization of phosphatidylserine and to DNA fragmentation, consistent with an apoptotic process involving the Fas pathway and mitochondrial dysfunction.[16,17] Cholesterol trafficking to ER membranes, resulting in activation of the CHOP arm of the UPR, was found to be the key signaling step in cholesterol-induced apoptosis in macrophages with the engagement of the type A scavenger receptor as a prerequisite.[18,19] Macrophage foam cell formation by an excessive accumulation of cholesteryl esters is an early event in the pathogenesis of atherosclerosis. Cholesteryl ester accumulation, however, does not induce apoptosis.[16] We have recently demonstrated that high intracellular triacylglycerol (TG) concentrations in macrophages from adipose triglyceride lipase-deficient (*Atgl–/–*) mice and in very low-density lipoprotein (VLDL)-loaded wild-type (Wt) macrophages trigger programmed cell death, involving mitochondrial dysfunction and activation of the mitochondrial apoptosis pathway.[20] ATGL catalyzes the initial step of TG hydrolysis in several tissues[21–23] including macrophages.[24] ATGL deficiency in mice results in increased fat mass because of an 80% reduction in TG hydrolase activity and a concomitant TG accumulation in cardiomyocytes, leading to heart failure and premature death.[25]

This study was designed to elucidate the mechanism responsible for programmed cell death in macrophages lacking ATGL. We provide evidence that increased ceramide synthesis triggers the mitochondrial apoptosis pathway resulting in mitochondrial dysfunction. Although ER stress still persists after inhibition of CerS activity by fumonisin B1 (FB1), *Atgl–/–* macrophages are rescued from apoptotic cell death. Our data suggest that predominantly mitochondria-based apoptotic signaling is implicated in programmed cell death of murine macrophages.

Results

TG accumulation triggers the UPR. To investigate whether ER stress (and concomitantly the UPR) might be implicated in apoptosis of *Atgl–/–* macrophages, we first determined the mRNA expression of the stress sensor Grp78/BiP. We found Grp78 mRNA to be significantly increased in *Atgl–/–* and VLDL-loaded Wt macrophages (2.0- and 2.5-fold, respectively) (Figure 1a). In addition, mRNA levels of other ER-resident chaperones (Pdi and Erdj4) were increased. As a consequence, we observed increased abundance of phosphorylated (p)PERK, which was not the case in untreated Wt macrophages (Figure 1b). Phosphorylation of the PERK substrate eukaryotic translation initiation factor (eIF)2α was increased by 2.9-fold in *Atgl–/–* and by 2.7-fold in VLDL-loaded Wt macrophages, respectively (Figure 1b). p-eIF2α generally shuts down synthesis of most cellular proteins, whereas the translation of the ATF4 transcription factor is specifically induced.[26] Accordingly, the protein expression of ATF4 was increased in the nuclear fractions of *Atgl–/–* and VLDL-loaded Wt macrophages (Figure 1c). Using immunofluorescence, we observed ATF4 to be located in the cytosol of Wt macrophages, whereas ATF4-specific staining was found in the nucleus of *Atgl–/–* and VLDL-loaded Wt macrophages (Figure 1d and Supplementary Figure S1), indicating the activation of ATF4. We next assessed ATF6 mRNA expression in all macrophages, which was increased in *Atgl–/–* and VLDL-loaded Wt macrophages (5.1- and 13.0-fold, respectively) (Supplementary Figure S2). Immunofluorescence analysis revealed ATF6 to be localized in the Golgi and nucleus of *Atgl–/–* and VLDL-loaded Wt macrophages but the lack of ATF6 translocation to the nucleus in Wt macrophages (Figure 1e and Supplementary Figure S3). One target of ATF4 and ATF6 activation is the CHOP promoter,[26] which appears to have a role in the induction of apoptosis during ER stress. CHOP protein expression was induced in both *Atgl–/–* and VLDL-loaded Wt macrophages but was absent in untreated Wt macrophages (Figure 1f). These findings indicate that the PERK/ATF4/ATF6 arm of the UPR is responsible for CHOP induction in *Atgl–/–* and VLDL-loaded Wt macrophages.

Lack of IRE-1α pathway activation in *Atgl–/–* macrophages. Next, we analyzed the protein expression of IRE1α as the third stress receptor. We found high IRE1α expression in *Atgl–/–* and VLDL-loaded Wt macrophages (Figure 2a). Generally, IRE1α phosphorylation activates XBP1 splicing. Surprisingly, we failed to detect any splicing of XBP1 in *Atgl–/–* and VLDL-loaded Wt macrophages (Figure 2b). Tunicamycin-treated Wt macrophages were used as positive control. XBP1 splicing depends on IRE1α phosphorylation and on the availability of XBP1 and ATF6. XBP1 mRNA was markedly reduced in *Atgl–/–* and VLDL-loaded Wt macrophages (Figure 2c). This finding suggests that the reduced abundance of XBP1 results in lack of XBP1 splicing. As a consequence, XBP1 itself is not involved in ER stress of *Atgl–/–* and VLDL-loaded Wt macrophages.

ATGL deficiency induces ceramide accumulation in macrophages. Studies in cancer cells defined ceramide as a biochemical mediator of ER stress.[27] We therefore determined ceramide concentrations in *Atgl–/–* and VLDL-loaded Wt macrophages. Although total ceramide levels were elevated, there was no significant change between *Atgl–/–,* VLDL-loaded Wt and Wt macrophages (Figure 3a). However, we observed a marked increase in C16:0 ceramide (Figure 3b). To analyze that ceramide synthase might be involved in the accumulation of C16:0 ceramide in *Atgl–/–*

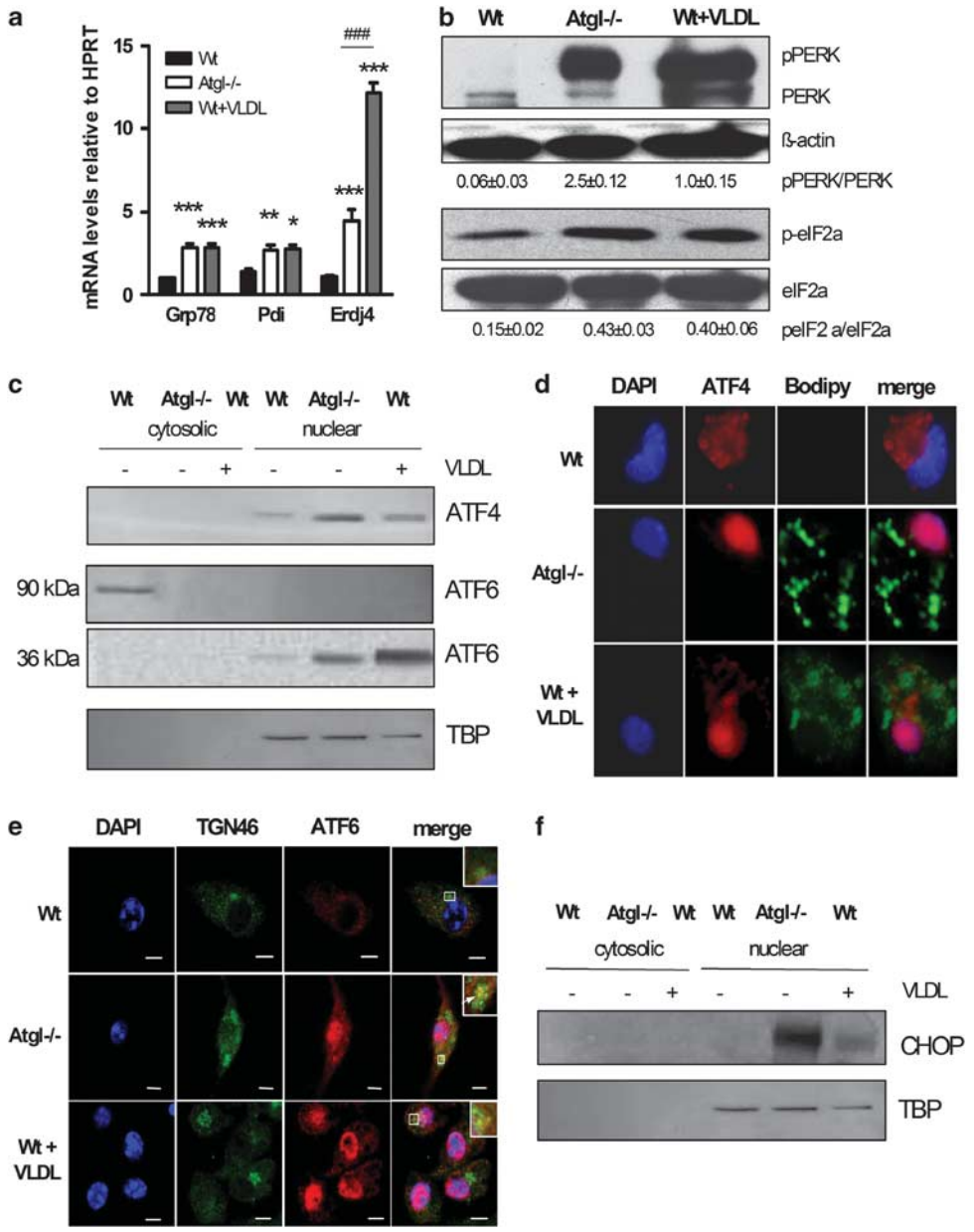

Figure 1 TG accumulation triggers ER stress via activation of the PERK and ATF6 pathways. (**a**) Total RNA was isolated from Wt, *Atgl–/–* and VLDL-loaded Wt macrophages. GRP78/BiP, Pdi and ERdj4 mRNA levels, including normalization to hypoxanthine-guanine phosphoribosyltransferase (HPRT), were determined by real-time PCR. Data are expressed as mean values ($n = 4$–6) of two independent experiments ± S.E.M. $^{*}P < 0.05$, $^{**}P \leq 0.01$, $^{***}P \leq 0.001$; $^{\#\#\#}P \leq 0.001$. (**b**) Cytosolic fractions (40 μg protein per lane) of Wt, *Atgl–/–* and VLDL-loaded Wt macrophages were resolved by SDS-PAGE and protein expression was analyzed using specific antibodies against PERK and eIF2α. The expression of β-actin was used as loading control. Data are expressed as the ratios of pPERK/PERK and p-eIF2α/eIF2α from three independent experiments ± S.E.M. (**c**) Cytosolic (40 μg protein per lane) and nuclear fractions (35 μg protein per lane) of Wt, *Atgl–/–* and VLDL-loaded Wt macrophages were resolved by SDS-PAGE and protein expression of ATF4 and ATF6 was determined by western blotting. TATA-binding protein (TBP) was used as nuclear fraction marker. (**d**) ATF4 and (**e**) ATF6 processing was analyzed after fixing and incubating the macrophages with specific antibodies. (**d**) Lipid droplets were stained with BODIPY 493/503. (**e**) Anti-TGN46 antibody was used as Golgi marker. (**d** and **e**) Cells were incubated with anti-rabbit Alexa-Fluor594 antibody and mounted in Vectashield/DAPI to visualize the nucleus. Representative images taken by fluorescence microscopy are shown. (**f**) CHOP protein expression was determined in nuclear fractions of Wt, *Atgl–/–* and VLDL-loaded Wt macrophages. TBP was used as nuclear fraction marker

macrophages, we determined mRNA levels of CerS1, 2, 4, 5 and 6. CerS1 was not expressed in macrophages. CerS2 mRNA expression was not significantly changed between the cells. Although CerS5 and CerS6 expression were more associated with C16:0 ceramide levels than CerS4 *in vitro*,[6] we observed mRNA levels of CerS4, 5 and 6 to be highly increased in *Atgl–/–* (8.4-, 11.9- and 15.6-fold, respectively) and VLDL-loaded Wt (3.9-, 8.0- and 5.4-fold, respectively) compared with untreated Wt macrophages (Figure 3c). In contrast, mRNA levels of acid ceramidase (Asah1) were markedly decreased in *Atgl–/–* and VLDL-loaded Wt macrophages (98% and 62%, respectively) (Figure 3d).

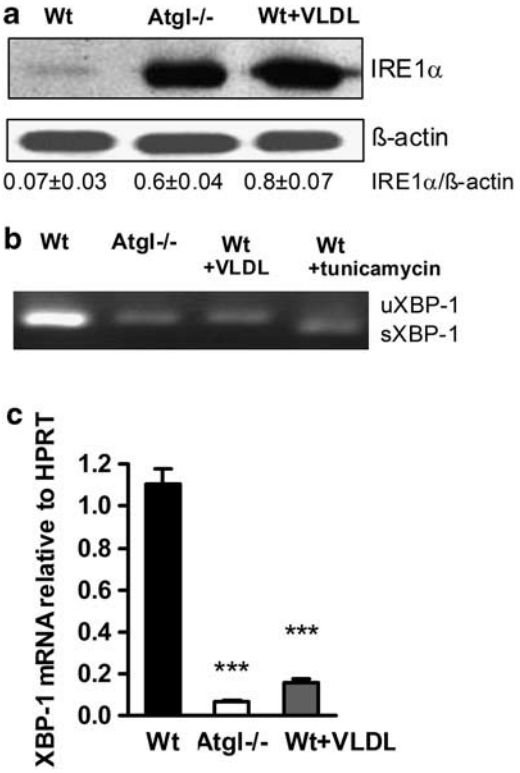

Figure 2 IRE-1α pathway fails to be activated in *Atgl–/–* macrophages. (**a**) Cytosolic fractions (40 μg protein per lane) from Wt, *Atgl–/–* and VLDL-loaded Wt macrophages were resolved by SDS-PAGE. Protein expression of IRE1α was analyzed by western blotting. Data are expressed as the ratio of IRE1α/β-actin from two independent experiments ± S.E.M. (**b**) RT-PCR analysis of unspliced (u) and spliced (s) XBP1 was performed in Wt, *Atgl–/–* and VLDL-loaded Wt macrophages. Tunicamycin-treated Wt macrophages were used as positive control. (**c**) XBP1 mRNA expression, including normalization to hypoxanthine-guanine phosphoribosyltransferase (HPRT), was determined by real-time PCR. ***$P \leq 0.001$

The abundance of neutral ceramidase (Asah2) was not significantly changed in *Atgl–/–* and VLDL-loaded Wt macrophages. These data indicate that both increased ceramide synthesis and reduced ceramide catabolism are involved in increased ceramide concentrations in *Atgl–/–* macrophages.

As ceramide accumulation is known to have an impact on the MAPK pathway, we determined p38 and Akt phosphorylation in Wt, *Atgl–/–* and VLDL-loaded Wt macrophages. We found comparable protein expression of total p38 and Akt in all macrophages, whereas phosphorylation of p38 and Akt was markedly decreased in *Atgl–/–* and VLDL-loaded Wt compared with untreated Wt macrophages (Figure 3e).

Overexpression of ceramide synthases increases C16:0 ceramide concentration and induces apoptosis in Wt macrophages. To elucidate that CerS might be involved in C16:0 ceramide accumulation in *Atgl–/–* macrophages, we transfected bone marrow-derived macrophages from Wt mice with CerS recombinant proteins. To analyze transfection efficiencies we determined CerS4, 5 and 6 mRNA levels. Although mRNA expression of all CerS enzymes was highly upregulated between 2400- and 36 000-fold (Figure 4a), total ceramide concentrations were significantly increased only in CerS4-transfected Wt macrophages by 2.8-fold (Figure 4b). C16:0 ceramide, however, was specifically elevated in macrophages overexpressing CerS4, 5 and 6 (4.1-, 3.7- and 6.6-fold, respectively). C24:2 ceramide was significantly increased in macrophages overexpressing CerS4 by 5.4-fold, whereas CerS5 and CerS6-transfected cells showed elevated C24:2 levels lacking statistical significance (Figure 4c). The number of apoptotic cells was significantly higher in all CerS-overexpressing cells compared with mock-transfected macrophages (Figure 4d and Supplementary Figure S4). Overexpression of CerS4 increased the amount of annexin V-positive, annexin V/propidium iodide (PI)-positive and necrotic PI-positive cells. CerS5-transfected cells showed a drastic increase in annexin V- and PI-positive macrophages but lacked an increase in annexin V/PI-positive cells. Overexpression of CerS6 led to significantly elevated number of annexin V- and annexin V/PI-positive macrophages (Figure 4d). Overexpression of each CerS resulted in markedly increased BAX and decreased BCL2 protein expression levels (Figure 4e). These data indicate that CerS4, 5 and 6 are involved in mitochondrial apoptosis of murine macrophages by an increased ceramide production of particularly C16:0 ceramide.

Inhibition of C16:0 ceramide accumulation rescues *Atgl–/–* macrophages from apoptotic cell death. To elucidate the impact of ceramide synthases on apoptosis in *Atgl–/–* macrophages, we inhibited ceramide synthesis by treating the cells with FB1 and determined annexin V and PI co-staining. In macrophages from Wt mice, we found 2.5% annexin V-positive cells indicative of cells undergoing apoptosis, whereas comparable with our previous observations[20] *Atgl–/–* macrophages exhibited 9.6% apoptotic cells (Figure 5a). Treatment of *Atgl–/–* macrophages with FB1 mainly rescued the apoptotic phenotype resulting in 4.1% apoptotic cells. The number of PI-positive cells, however, was unchanged in FB1– compared with untreated *Atgl–/–* macrophages (Figure 5a). Total ceramide concentrations were unchanged showing comparable amounts in Wt, *Atgl–/–* and FB1-treated *Atgl–/–* macrophages (Figure 5b). Notably, C16:0 ceramide was decreased by 56% in FB1-treated compared with untreated *Atgl–/–* macrophages, reaching similar levels as Wt macrophages (Figure 5c). C22:0, C24:0, C24:1 and C24:2 ceramide levels were comparable to the levels in Wt macrophages. C18:0 ceramide, however, was markedly higher in *Atgl–/–* macrophages after FB1 treatment. mRNA levels of CerS4, 5 and 6 were significantly reduced in FB1-treated compared with untreated *Atgl–/–* macrophages and were comparable to mRNA expression in Wt macrophages (Figure 5d). As TG concentrations were unaffected by FB1 treatment (Figure 5e), we conclude that TG themselves are not lipotoxic but the increased formation of ceramides (specifically C16:0 ceramide) leads to apoptotic cell death in *Atgl–/–* and VLDL-loaded Wt macrophages.

Inhibition of ceramide synthesis does not modulate ER stress in *Atgl–/–* macrophages. To assess the impact of

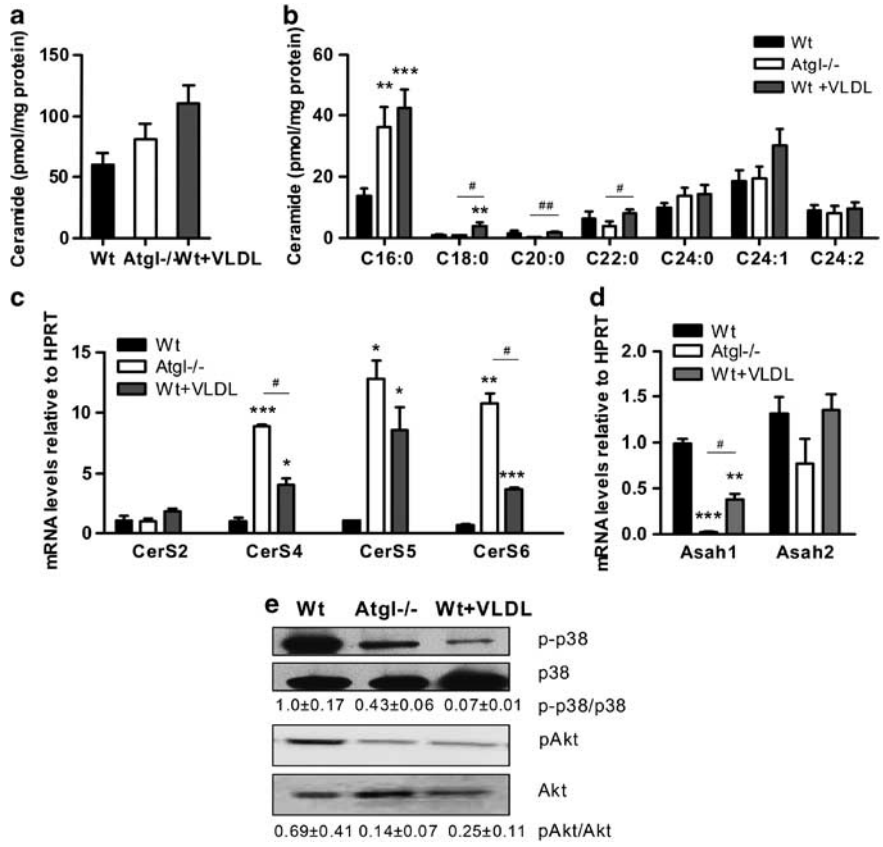

Figure 3 Ceramide accumulation in TG-rich macrophages. Concentrations of (**a**) total ceramide and (**b**) ceramide species in Wt, *Atgl–/–* and VLDL-loaded Wt macrophages were assessed by LC/MS. Data are expressed as means ($n=7$–9) of two independent experiments ± S.E.M. $^{**}P\leq0.01$, $^{***}P\leq0.001$; $^{\#}P<0.05$, $^{\#\#}P\leq0.01$. mRNA expression levels of (**c**) CerS2, 4, 5 and 6, and (**d**) Asah1 and Asah2, including normalization to hypoxanthine-guanine phosphoribosyltransferase (HPRT), were determined by real-time PCR. Data are expressed as means ($n=3$) of two independent experiments ± S.E.M. $^{*}P<0.05$, $^{**}P\leq0.01$, $^{***}P\leq0.001$; $^{\#}P<0.05$. (**e**) Western blot analysis in macrophage lysates from Wt, *Atgl–/–* and VLDL-loaded Wt macrophages using specific antibodies for total and phosphorylated (p) p38 and Akt. Protein expression of pAkt and p-p38 were quantified relative to total protein expression. Data are presented as means of two independent experiments ± S.E.M.

ceramide accumulation on ER stress in *Atgl–/–* macrophages, we investigated GRP78/BiP mRNA levels, the activation of eIF2α and IRE1α and the protein expression of CHOP after incubation with FB1. As shown in Figure 6a, GRP78/BiP mRNA expression was similarly elevated in untreated and FB1-treated *Atgl–/–* compared with Wt macrophages. Although still activated, quantification of western blotting experiments revealed that the presence of FB1 resulted in reduced phosphorylation of eIF2α and less IRE1α protein expression compared with untreated *Atgl–/–* macrophages (Figure 6b). CHOP protein expression was still induced in FB1-loaded *Atgl–/–* macrophages. These results indicate that inhibition of ceramide synthesis is unsuccessful in complete attenuation of ER stress in *Atgl–/–* macrophages.

As depletion of ER Ca^{2+} stores is a potent inducer of the UPR,[18,28] we explored whether disturbances of ER Ca^{2+} homeostasis are involved in the ER stress response of FB1-loaded *Atgl–/–* macrophages. The ER Ca^{2+} content of intact single Wt, *Atgl–/–* and FB1-treated *Atgl–/–* macrophages was visualized by measuring the cytosolic Ca^{2+} elevation in response to ER Ca^{2+} release using the sarcoplasmic/ER Ca^{2+} ATPase (SERCA) inhibitor 2,5-di-*t*-butyl-1,4-benzohydroquinone (BHQ) in Ca^{2+}-free medium. Cytosolic Ca^{2+} levels in FB1-treated *Atgl–/–* macrophages were lower than those in untreated *Atgl–/–* macrophages but were still substantially higher compared with Wt macrophages (Figure 6c). The ER Ca^{2+} content was reduced by 75% in *Atgl–/–* macrophages, whereas FB1-treated *Atgl–/–* macrophages showed comparable ER Ca^{2+} content as Wt macrophages (Figure 6d). In addition, basal Ca^{2+} concentrations, which were increased by 2.9-fold in *Atgl–/–* compared with Wt macrophages, were still 2.2-fold elevated in FB1-treated *Atgl–/–* macrophages (Figure 6e). These data indicate improved but still defective ER Ca^{2+} homeostasis in *Atgl–/–* macrophages after FB1 treatment, causing persistent ER stress.

Inhibition of ceramide accumulation rescues *Atgl–/–* macrophages from mitochondrial dysfunction. Next, we checked whether inhibition of the CerS enzymes by FB1 has an effect on mitochondrial dysfunction of *Atgl–/–* macrophages. For this purpose, we analyzed protein expression levels of pro-apoptotic BAX and anti-apoptotic BCL2. BAX expression and cytochrome *c* release were reduced and BCL2 expression was increased in FB1-treated *Atgl–/–* macrophages showing comparable expression levels

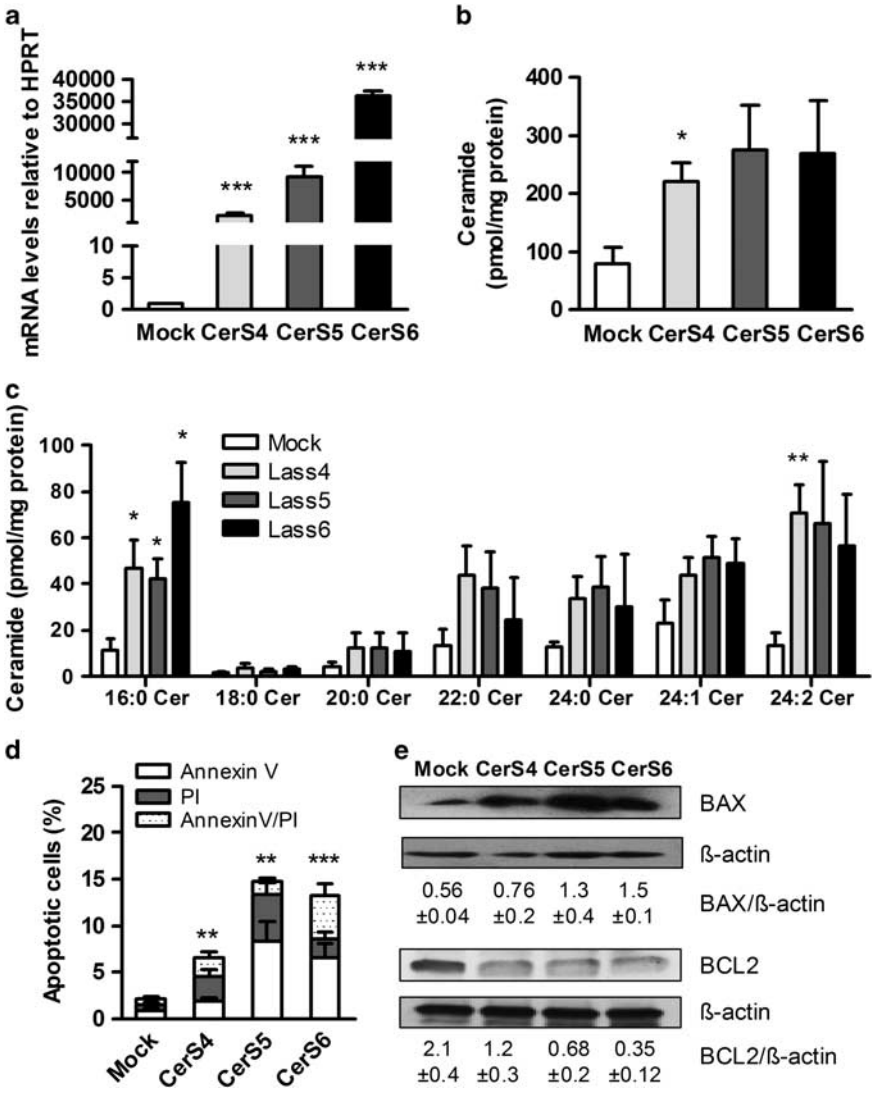

Figure 4 Overexpression of CerS4, 5 and 6 increases C16:0 ceramide and apoptotic cell death in Wt macrophages. Wt bone marrow-derived macrophages were transiently transfected with CerS4, 5 and 6. (**a**) mRNA expression of CerS4, 5 and 6 in transfected macrophages, including normalization to hypoxanthine-guanine phosphoribosyltransferase (HPRT), were determined by real-time PCR. Data are expressed as means of three independent experiments ± S.E.M. ***$P \leq 0.001$. (**b** and **c**) Ceramide concentrations in transfected macrophages were assessed by LC/MS. *$P < 0.05$, **$P \leq 0.01$. (**d**) Transfected macrophages were plated on glass coverslips. Apoptosis was assessed after co-staining with FITC-conjugated annexin V and PI, respectively, by fluorescence microscopy. Three fields of cells with ~300 cells per field were counted for each condition. Data are expressed as the mean percentage of total cells ± S.E.M. that stained with annexin and PI. **$P \leq 0.01$; ***$P \leq 0.001$. (**e**) Cytosolic fractions of transfected macrophages were isolated and proteins (40 μg per lane) were resolved by SDS-PAGE. Protein expressions of BAX and BCL2 using specific antibodies were determined by western blotting. Abundances of BAX and BCL2 were quantified relative to β-actin expression. Data are presented as means of two independent experiments ± S.E.M.

as Wt macrophages (Figure 7a). In addition, FB1 treatment was associated with increased mRNA levels of NADH/ubiquinone oxidoreductase (complex I) and decreased mRNA abundance of the NADPH oxidase activator (Noxa1), which triggers the generation of superoxide anion, compared with untreated *Atgl–/–* macrophages (Figure 7b). MitoTracker staining and electron microscopy displayed morphological changes in mitochondria compared with untreated *Atgl–/–* macrophages, in which mitochondria were fragmented and electron-light (Figure 7c). Quantification of the size revealed that mitochondria in *Atgl–/–* macrophages were 51% smaller than in Wt macrophages. This difference was totally abolished after incubation with FB1, which resulted in mitochondria of comparable size as observed in Wt macrophages (Figure 7d). These findings demonstrate that inhibition of ceramide synthesis by FB1 treatment eliminates mitochondrial dysfunction and mitochondrial apoptosis in *Atgl–/–* macrophages.

Discussion

Intracellular TG hydrolysis by ATGL is required to generate fatty acids,[24] which are transported across the mitochondrial membranes by carnitine–palmitoyl transferase 1 and

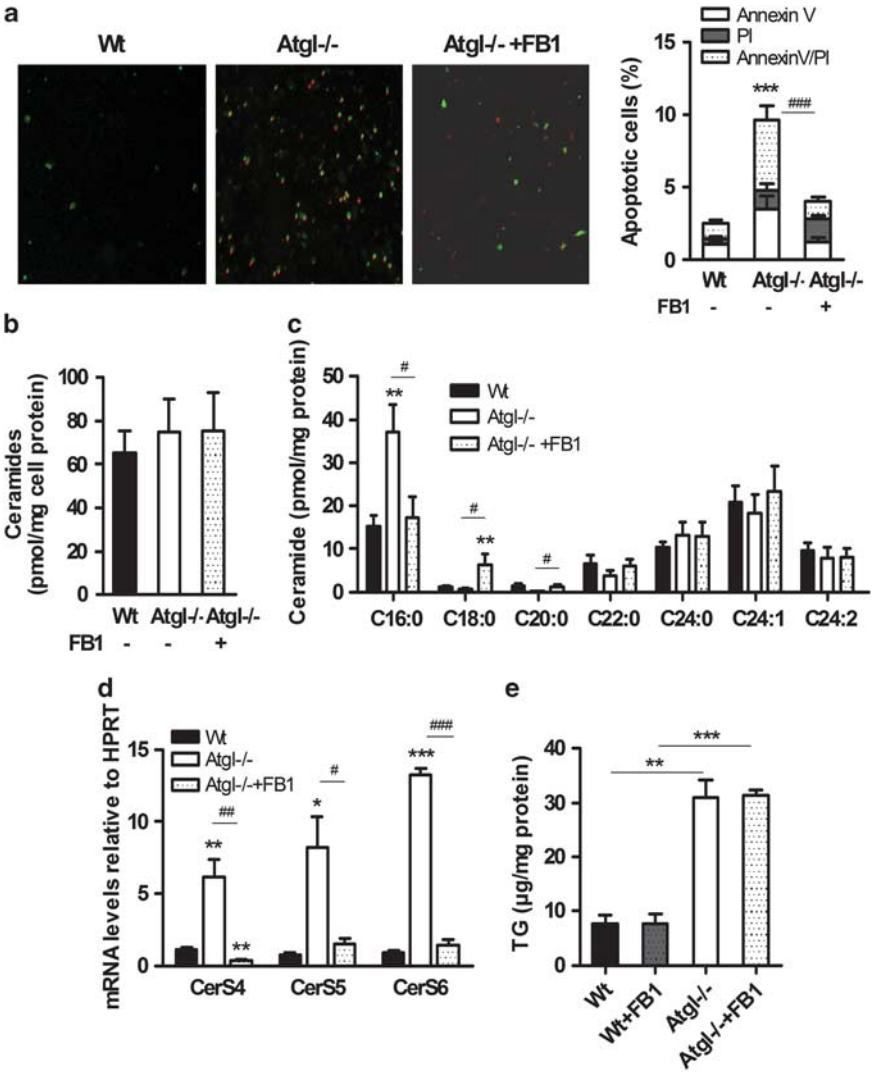

Figure 5 Inhibition of ceramide synthesis rescues *Atgl–/–* macrophages from programmed cell death. (**a**) Wt, *Atgl–/–* and *Atgl–/–* macrophages treated with FB1 (10 μg/ml, 12 h) were plated on glass coverslips. Apoptosis was assessed after co-staining with FITC-conjugated annexin V (green) and PI (red), respectively, by fluorescence microscopy. Original magnification, $\times$ 10. Three fields of cells with $\sim$700 cells per field were counted for each condition. Data are expressed as the mean percentage of total cells $\pm$ S.E.M. that stained with annexin and PI. $^{***}P \leq 0.001$; $^{\#\#\#}P \leq 0.001$. (**b**) Total ceramide and (**c**) ceramide species were measured by LC/MS. $^{**}P \leq 0.01$; $^{\#}P < 0.05$. (**d**) mRNA abundances of CerS4, 5 and 6, including normalization to hypoxanthine-guanine phosphoribosyltransferase (HPRT), were determined by real-time PCR. Data are expressed as means ($n = 3$–6) $\pm$ S.E.M. $^{*}P < 0.05$, $^{**}P \leq 0.01$, $^{***}P \leq 0.001$; $^{\#}P < 0.05$, $^{\#\#}P \leq 0.01$, $^{\#\#\#}P \leq 0.001$. (**e**) Intracellular TG concentrations were analyzed spectrophotometrically. $^{**}P \leq 0.01$, $^{***}P \leq 0.001$

carnitine. Once inside the mitochondria, fatty acids undergo β-oxidation to generate ATP. We suggest that insufficient fatty acid supply in *Atgl–/–* macrophages results in impaired mitochondrial function, leading to reactive oxygen species (ROS) generation. ROS are capable to act as second messenger and, for example, mediate apoptosis. Mitochondria have an essential role in Ca^{2+} signaling[29] and disruption of the mitochondrial membrane potential by genetic or metabolic stress causes elevated cytoplasmic Ca^{2+} levels as a consequence of the inability of these mitochondria to buffer Ca^{2+}.[30,31] Recently, Timmins *et al.*[32] revealed that the Fas pathway (through induction of the Fas receptor) and the mitochondrial pathway (through accumulation of mitochondrial Ca^{2+}) are linked via calcium/calmodulin-dependent protein kinase II in ER-stressed macrophages. We therefore hypothesized that apoptosis in *Atgl–/–* macrophages and in Wt macrophages loaded with VLDL was the consequence of activation of various apoptosis pathways.

Evaluation of UPR activation in *Atgl–/–* and VLDL-loaded Wt macrophages showed an induction of CHOP, indicating the accumulation of unfolded or misfolded proteins in the ER. Although the UPR is primarily an ER repair mechanism, CHOP triggers apoptosis in the absence of a functional cell repair.[18,33] The UPR starts when GRP78/BiP dissociates from PERK, IRE1 and ATF6, and instead binds to accumulating unfolded proteins.[34] Dissociation of GRP78/BiP results in PERK, IRE1 and ATF6 homodimerization and oligomerization to an active state, which as a consequence triggers apoptosis. *Atgl–/–* macrophages and VLDL-loaded Wt cells showed an increase in activated PERK, resulting in increased

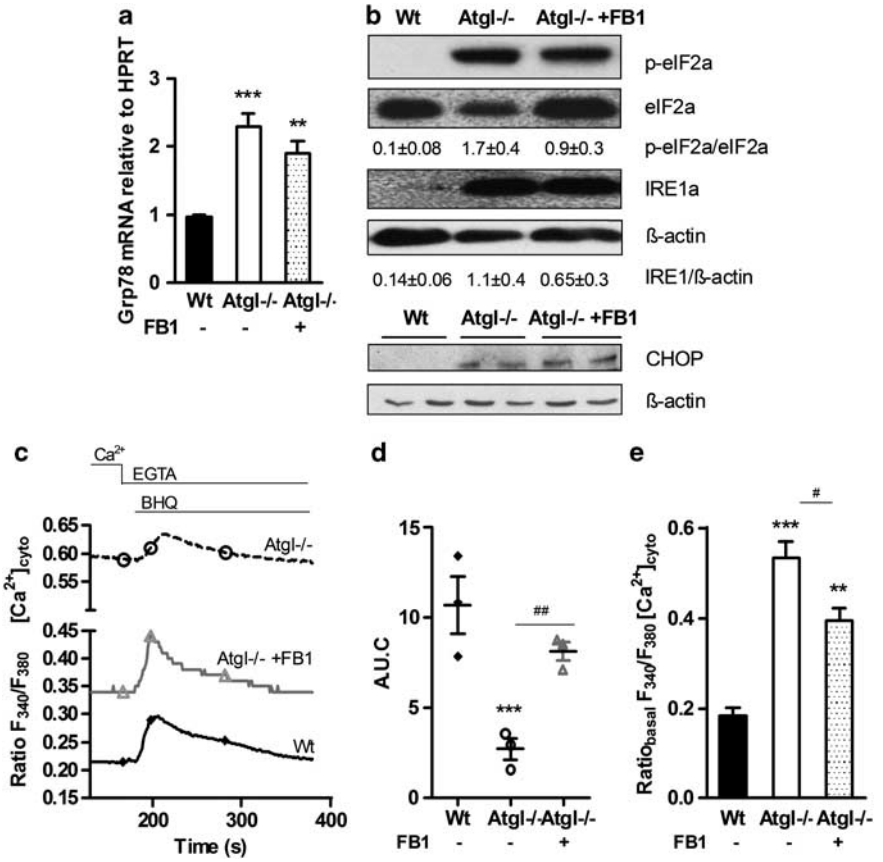

Figure 6 Persistent ER stress after inhibiting ceramide synthesis in *Atgl–/–* macrophages. (**a**) mRNA expression of Grp78/BiP in Wt, *Atgl–/–* and FB1-treated *Atgl–/–* macrophages, including normalization to hypoxanthine-guanine phosphoribosyltransferase (HPRT), was determined by real-time PCR. $^{**}P \leq 0.01$, $^{***}P \leq 0.001$. (**b**) Cytosolic fractions of macrophages were isolated and proteins were resolved by SDS-PAGE. Protein expression was determined using specific antibodies for phosphorylated (p)eIF2α, eIF2α, and IRE1α by western blotting. Data are expressed as the ratios of eIF2α/eIF2α and IRE1α/β-actin of two independent experiments ± S.E.M. CHOP protein expression was analyzed in whole cell lysates. The expression of β-actin was determined as loading control. (**c**) Wt, *Atgl–/–* and FB1-treated *Atgl–/–* macrophages were plated on coverslips in DMEM/10% LPDS. The fura-2 fluorescence ratio (340/380 nm) was determined in single macrophages before and after the addition of BHQ (15 mM) in the presence of 1 mM EGTA. Data are presented as mean values ± S.E.M. of 300 cells per genotype of three independent experiments. (**d**) Area under the curve after the addition of BHQ was calculated. Dots represent means of 300 cells of three independent experiments ± S.E.M. $^{***}P \leq 0.001$; $^{\#\#}P \leq 0.01$. (**e**) Basal cytosolic Ca^{2+} concentrations were calculated from the fura-2 fluorescence ratios (340/380 nm) during the initial 5 min. $^{**}P \leq 0.01$, $^{***}P \leq 0.001$; $^{\#}P < 0.05$

phosphorylation of eIF2α and subsequent nuclear CHOP protein expression. Translocation of ATF4 and ATF6 from the cytosol and/or Golgi to the nucleus demonstrates that these two arms of the UPR are activated in *Atgl–/–* macrophages. The protein expression of IRE1α was also highly increased in both *Atgl–/–* and VLDL-loaded Wt macrophages but failed to result in XBP1 splicing. In cells undergoing ER stress, oligomerization of IRE1 generally leads to trans-autophosphorylation and activation of its RNAse domain to excise a 26-nt sequence from uXBP1, producing mature sXBP1.[35] Our finding might be explained by the drastically reduced mRNA expression of uXBP1 in *Atgl–/–* and VLDL-loaded Wt macrophages. From these observations, we conclude that ER stress in macrophages is mainly depending on the activation of the PERK/ATF4 and ATF6 arms of the UPR, resulting in the induction of CHOP expression.

ER stress activation is frequently accompanied by depletion of ER Ca^{2+} stores as potent inducers of the UPR and Ca^{2+} release into the cytosol.[8,28] We therefore hypothesized that one possibility how high intracellular TG content may induce ER stress is the disturbance in Ca^{2+} homeostasis. Both Ca^{2+} overload and depletion of the ER Ca^{2+} pool can result in changes in protein folding and ER stress.[36] Basal cytosolic Ca^{2+} levels were markedly increased in *Atgl–/–* macrophages, whereas the ER Ca^{2+} content was reduced. As an interaction between signals from ceramide and Ca^{2+} exists in different cell types[37,38] and ceramide induces ER stress and apoptosis in human cancer cells,[27] we determined ceramide concentrations. Although total ceramide concentrations were comparable in Wt, *Atgl–/–* and VLDL-loaded Wt macrophages, we observed a specifically significant increase in C16:0 ceramide. *De novo*-generated C16 ceramide contributes to spontaneous neutrophil apoptosis by acting upstream of caspase-3 activation.[7] In Ramos B cells, *de novo*-generated C16 ceramide is involved in mitochondrial damage, resulting in downstream activation of caspases and apoptosis.[39] Overexpression of either CerS4, 5 or 6 resulted in increased BAX protein levels in murine Wt macrophages, whereas BCL2 protein expression was decreased. C16:0 ceramide concentrations were markedly increased compared

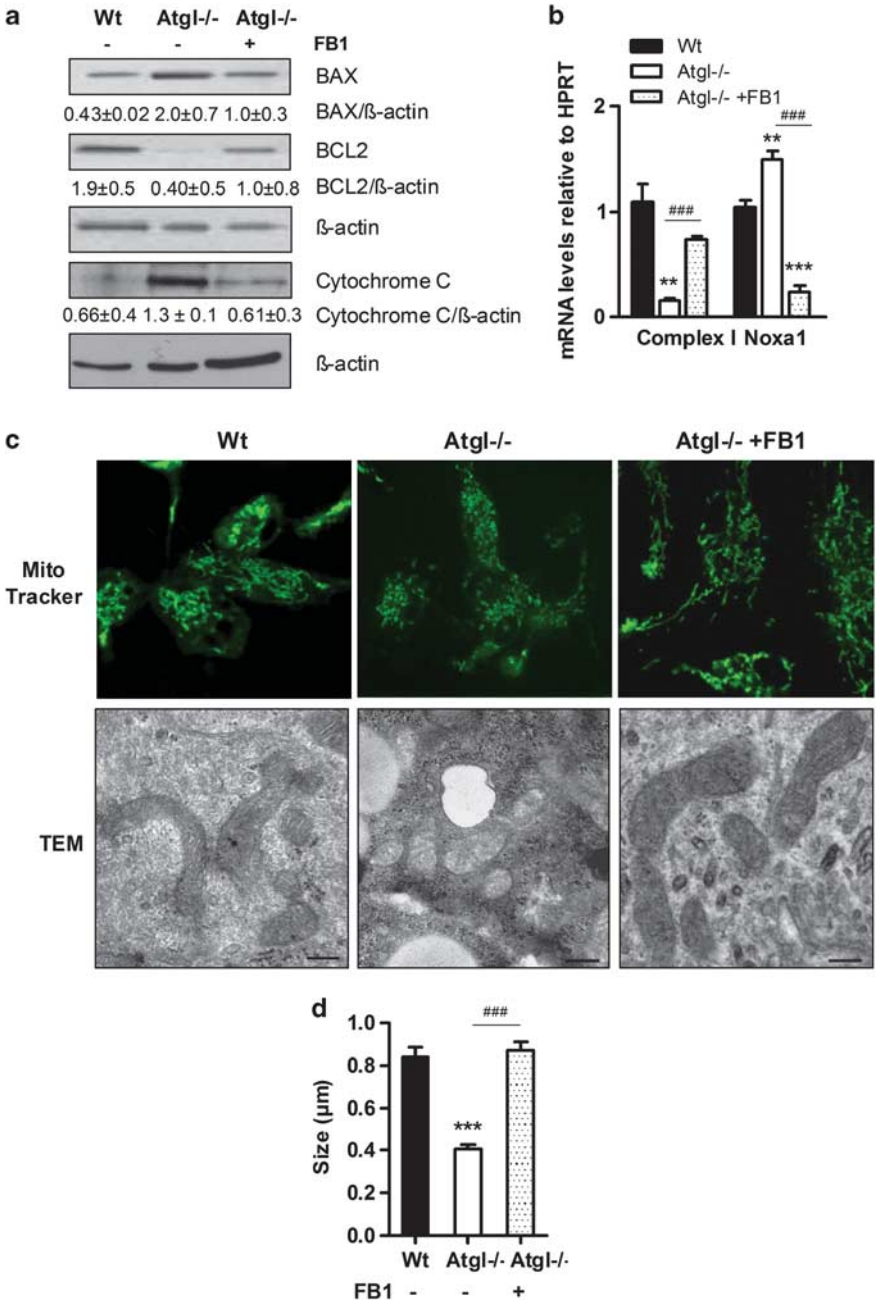

Figure 7 Inhibition of ceramide synthesis eliminates mitochondrial apoptosis and mitochondrial dysfunction in *Atgl–/–* macrophages. (**a**) BAX, BCL2 and cytochrome *c* protein levels in cytosolic fractions of Wt, *Atgl–/–* and FB1-treated *Atgl–/–* macrophages were assessed by western blotting. Data are presented as the ratios of the protein expressions relative to β-actin of two independent experiments ± S.E.M. (**b**) NADH/ubiquinone oxidoreductase (complex I) and Noxa1 mRNA levels including normalization to hypoxanthine-guanine phosphoribosyltransferase (HPRT) were determined in Wt, *Atgl–/–* and FB1-treated *Atgl–/–* macrophages by real-time PCR. Data are expressed as mean values ($n = 3$–5) ± S.E.M. $^{**}P \leq 0.01$, $^{***}P \leq 0.001$; $^{\#\#\#}P \leq 0.001$. (**c**) Mitochondrial morphology of Wt, *Atgl–/–* and FB1-treated *Atgl–/–* macrophages. Upper row: representative confocal laser-scanning microscopy images after green MitoTracker staining are shown. Lower row: representative electron micrographs. Scale bars: 0.2 μm. (**d**) Size quantification of mitochondria visualized by electron microscopy. Data are expressed as mean ($n = 45$–48) ± S.E.M. $^{***}P \leq 0.001$; $^{\#\#\#}P \leq 0.001$

with mock-transfected Wt macrophages and were similar or even higher when compared with *Atgl–/–* macrophages. Accordingly, we observed an increased amount of apoptotic and necrotic cells compared with mock-transfected macrophages. The number of dead cells, however, lacks a direct association with mRNA expression levels of CerS4, 5 and 6. This discrepancy might be explained by differences between mRNA levels and protein expression and/or activity. As overexpression of either CerS resulted in increased C16:0 ceramide and apoptosis with induced BAX and reduced BCL2 expression, we conclude that C16:0 ceramide is the apoptotic trigger in murine macrophages.

C16 ceramide may also augment the execution of apoptosis by the inactivation of pro-survival pathways.

Ceramide has been shown to activate ceramide-activated protein phosphatase leading to the dephosphorylation of Akt,[40] which may have profound effects on the activities of downstream factors implicated in the regulation of apoptosis. By activation of ceramide-activated protein phosphatase, ceramide negatively regulates pro-growth kinases such as p38.[41] Phosphorylation of both Akt and p38 were markedly reduced in *Atgl–/–* and VLDL-loaded Wt macrophages, suggesting that these kinases are indirectly inhibited by increased C16:0 ceramide concentrations in these cells.

Treatment with FB1, which we used as an inhibitor for ceramide synthesis, normalized the mRNA levels of CerS4, 5 and 6 in *Atgl–/–* macrophages and decreased the amount of C16:0 ceramide to Wt levels. This reduction was accompanied by rescue of *Atgl–/–* macrophages from apoptotic cell death, as indicated by a decrease in externalization of phosphatidylserine, BAX protein expression and cytochrome *c* release and an increase in BCL2 protein expression. The amount of PI-positive cells, however, was unaffected by FB1 treatment, suggesting that a small amount of cells are still prone to necrosis. This might, at least in part, be due to the still persisting ER stress in FB1-treated *Atgl–/–* macrophages with remaining eIF2α and IRE1α activation. As ceramide synthase inhibition by FB1 treatment reduced but failed to abolish ER stress, we conclude that other mediators of ER stress must be present in *Atgl–/–* macrophages. One possible explanation might be defective Ca^{2+} homeostasis in FB1-treated *Atgl–/–* macrophages as revealed by substantially higher basal cytosolic Ca^{2+} levels compared with Wt macrophages. We therefore hypothesize that disturbances of ER Ca^{2+} homeostasis are involved in the ER stress response of FB1-loaded *Atgl–/–* macrophages. Our results suggest that ER stress itself is not the trigger of apoptotic cell death in *Atgl–/–* macrophages because FB1 treatment rescued the cells from programmed cell death without eliminating ER stress responses. Our data indicate that C16:0 is essential and sufficient for TG-mediated mitoapoptosis. Although the exact mechanism is still elusive, we hypothesize that the absence of ATGL or the presence of high concentrations of VLDL leads to a shift in ceramide metabolism, resulting in increased sphingosine formation, which is catabolized to C16:0 ceramide within mitochondria.[42] The increased concentration of C16:0 in the mitochondria then leads to apoptotic cell death in *Atgl–/–* and VLDL-loaded Wt macrophages. Importantly, our data demonstrate that FB1 treatment of *Atgl–/–* macrophages rescued the cells from mitochondrial dysfunction, indicating that inhibition of C16:0 ceramide synthesis is sufficient to cure *Atgl–/–* macrophages from programmed cell death.

Materials and Methods

Animal studies. *Atgl–/–* mice were generated and genotyped as described elsewhere.[25] Wt and *Atgl–/–* mice were kept on a standard chow diet (4.5% w/w fat; Ssniff, Soest, Germany) on a regular 12-h dark–light cycle. All studies were performed with male *Atgl–/–* mice and Wt littermates backcrossed at least seven times on a C57Bl/6 genetic background. Animal experiments were performed in accordance with the standards established by the Austrian Federal Ministry of Science and Research, Division of Genetic Engineering and Animal Experiments (Vienna, Austria).

Cell culture. Macrophages were harvested from the peritoneum of 8- to 10-week-old male *Atgl–/–* and Wt mice 3 days after intraperitoneal injection of 2.5 ml 3% thioglycolate medium. Cells were transferred into six-well dishes containing Dulbecco's modified Eagle's medium (DMEM) (Gibco, Invitrogen, Vienna, Austria). After 2 h, non-adherent cells were aspirated, adherent macrophages were washed three times with PBS and cultivated in DMEM containing 10% lipoprotein-deficient serum (LPDS) and 100 μg/ml penicillin/streptomycin for 24 h. Wt macrophages were incubated with 150 μg VLDL/ml for 24 h. VLDL was isolated from human plasma by density gradient ultracentrifugation.[43] To inhibit ceramide synthesis, *Atgl–/–* macrophages were treated with 10 μM FB1 (Calbiochem, Darmstadt, Germany) for 12 h.

TG concentrations in macrophages. Lipids from macrophages were extracted as described.[24] TG concentrations in 25 μl aliquots were determined enzymatically (Diagnostic Systems, Holzheim, Germany).

Real-time PCR. Total RNA was isolated from macrophages using peqGOLD kit (PeqLab, Vienna, Austria) according to the manufacturer's instructions. Two μg of total RNA were reverse transcribed using the High Capacity cDNA Reverse Transcription Kit (Applied Biosystems, Vienna, Austria). Quantitative real-time PCR was performed on an ABI prism 7900 real-time PCR instrument (Applied Biosystems) using the QuantiFast SYBR Green PCR kit (Qiagen, Hilden, Germany). Primer sequences are available on request. Data are displayed as expression ratios of genes of interest normalized to the expression of hypoxanthine-guanine phosphoribosyltransferase as internal reference in each sample. Quantitative real-time PCR data were analyzed by the 2^{-ddCt} method.

Isolation of cytosolic and nuclear fractions. Mitochondria- and nucleus-free cytosolic fractions of macrophages were isolated using Benchtop mitochondria isolation kit (MitoSciences, Eugene, OR, USA) according to the manufacturer's instructions. Cytosolic and nuclear extracts were prepared by resuspending the cells in a buffer containing 10 mM HEPES pH7.9, 50 mM NaCl, 0.1 mM EDTA, 0.5 M sucrose, 0.5% Triton X-100, 1 mM DTT, 100 mM NaF, 1 mM PMSF, 4 μg/ml aprotinin and 2 μg/ml pepstatin. After 5-min incubation on ice, the lysates were centrifuged at 1 000 r.p.m. for 10 min. The supernatant was centrifuged at 14 000 r.p.m. for 15 min. The supernatant (cytosolic fraction) was used to detect to detect BAX, BCL2, cytochrome *c*, p-eIF2α, eIF2α, PERK and IRE-1. The pellet from the 1 000 r.p.m. centrifugation step was washed with washing buffer (10 mM HEPES pH 7.9, 10 mM KCl, 0.1 mM EDTA, 0.1 mM EGTA, 1 mM DTT, 1 mM PMSF, 4 μg/ml aprotinin and 2 μg/ml pepstatin). Thereafter, the pellet was resuspended in a buffer containing 10 mM HEPES pH 7.9, 50 mM NaCl, 0.1 mM EDTA, 0.1 mM EGTA, 0.1% NP40, 1 mM DTT, 1 mM PMSF, 4 μg/ml aprotinin and 2 μg/ml pepstatin and centrifuged at 14 000 r.p.m. for 10 min at 4 °C. The supernatant containing nuclear proteins was used to detect CHOP, ATF4 and ATF6. Anti-TBP antibody was used as nuclear marker 14 000 r.p.m. for 15 min. The supernatant (cytosolic fraction) was used.

Western blotting analysis. A total of 40 μg of cytosolic and 35 μg of nuclear fractions were separated on 12.5% or 18% SDS polyacrylamide gel by electrophoresis and electroblotted onto nitrocellulose protran BA85 membranes (Whatman, Vienna, Austria). The blots were blocked in 5% BSA plus 0.1% Tween-20 and incubated with the following primary polyclonal antibodies (if not stated otherwise): anti-rabbit PERK (1 : 500), eIF2α (1 : 1000), p-eIF2α (1 : 1000), IRE1α (1 : 800), monoclonal anti-mouse CHOP (1 : 500), BAX (1 : 1000), BCL2 (1 : 1000), cytochrome *c* (1 : 1000) (all purchased from Cell Signaling Technology, Danvers, MA, USA), ATF4 (1 : 1000), ATF6 (1 : 1000), TBP (1 : 1000) (Abcam, Cambridge, UK) and monoclonal anti-mouse β-actin (1 : 1000) (Santa Cruz Biotechnology, Heidelberg, Germany). All blots were incubated overnight at 4 °C. The horseradish peroxidase-conjugated goat anti-rabbit (1 :5000) (Santa Cruz Biotechnology) and rabbit anti-mouse antibodies (1 : 1000) (Dako, Glostrup, Denmark) were visualized by enhanced chemiluminescence detection (ECL Plus; Amersham Biosciences, Piscataway, NJ, USA) on an AGFA Curix Ultra X-Ray film (Siemens, Graz, Austria).

Apoptosis assay. Apoptosis in Wt, *Atgl–/–*, VLDL-loaded Wt and FB1-treated *Atgl–/–*macrophages cells was assayed by annexin V and PI co-staining using Annexin-V-FLUOS Staining Kit (Roche, Vienna, Austria) as described.[20] Pictures were taken by fluorescence microscopy (Zeiss Axioskop; Carl Zeiss GmbH, Vienna, Austria) equipped with a 10X objective and filters appropriate for fluorescein (annexin V) and rhodamine (PI). For quantification, three fields of cells for each condition were counted. The number of annexin V/PI-positive cells in each field is expressed as the percentage of these cells per total cells counted.

Immunohistochemistry. Wt and *Atgl*–/– macrophages were fixed with 4% formaldehyde in PBS for 30 min at room temperature. Cells were blocked with PBS containing 2% donkey serum, 100 mM glycine and 0.1% saponin for 2 h. Thereafter, cells were incubated with anti-ATF4 (1 : 300), anti-ATF6 (1 : 500) and anti-TGN46 (1 : 150) (Abcam) for 2 h. For visualization, the cells were incubated with donkey anti-mouse or rabbit secondary antibodies conjugated to AlexaFluor-555 (1 : 250) or anti-ship 488 (1 : 300) (Molecular Probes, Invitrogen, Vienna, Austria) for 1 h. After washing the cells with PBS they were mounted in Vectashield/DAPI (Vector Laboratories, Burlingame, CA, USA). Images were taken on a confocal Zeiss 510 META confocal laser scanning microscope (Carl Zeiss Microimaging Inc., Thornwood, NY, USA).

Ceramide measurements. Macrophages from Wt mice in the absence or presence of VLDL (150 μg/ml) and macrophages from *Atgl*–/– mice in the absence and presence of FB1 (10 μM for 12 h) were cultured in 12-well plates in DMEM at $\sim$80% confluence. The cells were washed twice with PBS and scraped with 500 μl PBS. After centrifugation (5 min at 5 000 r.p.m.), the pellet was resuspended in chloroform/methanol/water/pyridin (60 : 30 : 6 : 1, v : v : v : v). Ceramides were extracted by incubating the samples at 37 °C for 24 h in a shaking water bath. Denatured proteins were removed by passing the samples through cotton wadding. The solvent was evaporated under a stream of nitrogen. The pellets were dissolved in 2.5 ml methanol and NaOH was added to a final concentration of 100 mM. After shaking for 2 h at 37 °C, samples were neutralized by the addition of 10 μl concentrated acetic acid. Finally, the solvent was evaporated under a stream of nitrogen. The extract was dissolved in 50 μl chloroform. Chloroform was evaporated under a stream of nitrogen and the lipids were redissolved in 50 μl chloroform/methanol (1 : 1, v : v) for HPLC-MS/MS analysis. For quantitation 20 pmol C17:0 ceramide per sample was added as internal standard during resuspending the cells. Chromatographic separation of ceramides was performed by an Accela HPLC (Thermo Scientific, San Jose, CA, USA) on a Thermo Hypersil GOLD C18, 100 $\times$ 1 mm, 1.9 μm column using solvent A (1% ammonium acetate (v/v) and 0.1% formic acid (v/v) in H_2O) and solvent B (acetonitrile/2-propanol (5 : 2, v/v) supplemented with 1% ammonium acetate (v/v) and 0.1% formic acid (v/v)). The gradient was run from 35 to 70% B for 4 min, then to 100% B for additional 16 min with subsequent hold at 100% for 10 min. The flow rate was 250 μl/min. Ceramides were analyzed by a precursor ion scan of m/z 264 at a collision energy of 30 eV using a TSQ Quantum Ultra LC/MS/MS (Thermo Scientific).

Transfection of murine macrophages. Bone marrow-derived cells were collected from Wt femurs and tibias by flushing the bones with sterile medium (DMEM, 10% LPDS, 50 μg/ml penicillin and 50 μg/ml streptomycin). The cells were washed extensively and resuspended in medium containing 10 ng/ml macrophage colony-stimulating factor (M-CSF) (R&D system, Vienna, Austria) to differentiate monocytes into macrophages. After 3 days, the cells were washed carefully with PBS. The homogeneity of the population was determined by FACS analysis (FACSCalibur flow cytometer; BD Biosciences, San Jose, CA, USA) using F4/80 antibody (eBioscience, Vienna, Austria). Transfection was performed at the third day of differentiation using jetPEI-Macrophage (Polyplus-transfection SA, Illkirch, France) in the presence of serum and M-CSF according to the manufacturer's instruction. Plasmids containing full-length cDNAs of CerS4 (in pCMV-SPORT6), CerS5 (in pYX-Asc) and CerS6 (in pCMV-SPORT6) were purchased from Invitrogen.

Cytosolic Ca^{2+} measurements. Cells grown on coverslips in six-well dishes were loaded with 4 μM fura-2 (Molecular Probes, Eugene, OR, USA) and sulphinpyrazone (250 μM) (Sigma-Aldrich, Vienna, Austria) at room temperature for 30 min as described.[18,20] After 100 s, 15 μM of the SERCA inhibitor BHQ was added to empty endoplasmic Ca^{2+} pools into the cytosol. Fluorescence images (510 nm emission after alternate 340 and 380 nm excitation) of 300 cells were collected by fluorescence microscopy. Each image was corrected for background fluorescence and the 340 : 380 nm fluorescence ratios of individual cells were calculated.

Mitochondria and lipid droplet staining. Mitochondria of Wt, *Atgl*–/– and FB1-treated *Atgl*–/– macrophages were stained with 0.5 μM MitoTracker Green (Molecular Probes, Invitrogen) (37 °C, 5 min). Lipid droplets were visualized using Nile Red (2.5 μg/ml) staining. Z-stacks were recorded using a Leica SP5 AOBS confocal microscope (Leica Microsystems, Vienna, Austria).

Statistics. Statistical analyses were performed using GraphPad Prism 5.0 software (GraphPad Software, La Jolla, CA, USA). The significance of paired data was determined by Student's *t*-test. Data with >2 groups or ≥ 2 independent variables were analyzed by ANOVA, followed by the Bonferroni *post-hoc* test. Significance levels were set at $^{*}P<0.05$,$^{**}P\leq 0.01$ and $^{***}P\leq 0.001$.

Conflict of Interest

The authors declare no conflict of interest.

Acknowledgements. This work was supported by the Medical University of Graz (PhD Program Molecular Medicine), the Austrian Science Fund FWF (SFB-LIPOTOX F30, DK-MCD W1226, P19186, and P22832), and the Austrian Federal Ministry of Science and Research (GEN-AU project Genomics of Lipid-associated Disorders – GOLD). EA and PD were funded by the PhD Program Molecular Medicine of the Medical University of Graz. We thank A Ibovnik for excellent technical assistance and I Hindler for mice care.

1. Ogretmen B, Hannun YA. Biologically active sphingolipids in cancer pathogenesis and treatment. *Nat Rev Cancer* 2004; **4**: 604–616.
2. Futerman AH, Stieger B, Hubbard AL, Pagano RE. Sphingomyelin synthesis in rat liver occurs predominantly at the cis and medial cisternae of the Golgi apparatus. *J Biol Chem* 1990; **265**: 8650–8657.
3. Kolter T, Proia RL, Sandhoff K. Combinatorial ganglioside biosynthesis. *J Biol Chem* 2002; **277**: 25859–25862.
4. Guillas I, Jiang JC, Vionnet C, Roubaty C, Uldry D, Chuard R *et al.* Human homologues of LAG1 reconstitute Acyl-CoA-dependent ceramide synthesis in yeast. *J Biol Chem* 2003; **278**: 37083–37091.
5. Guillas I, Kirchman PA, Chuard R, Pfefferli M, Jiang JC, Jazwinski SM *et al.* C26-CoA-dependent ceramide synthesis of Saccharomyces cerevisiae is operated by Lag1p and Lac1p. *EMBO J* 2001; **20**: 2655–2665.
6. Mizutani Y, Kihara A, Igarashi Y. Mammalian Lass6 and its related family members regulate synthesis of specific ceramides. *Biochem J* 2005; **390**: 263–271.
7. Seumois G, Fillet M, Gillet L, Faccinetto C, Desmet C, Francois C *et al. De novo* C16- and C24-ceramide generation contributes to spontaneous neutrophil apoptosis. *J Leukoc Biol* 2007; **81**: 1477–1486.
8. Szegezdi E, Logue SE, Gorman AM, Samali A. Mediators of endoplasmic reticulum stress-induced apoptosis. *EMBO Rep* 2006; **7**: 880–885.
9. Ron D, Walter P. Signal integration in the endoplasmic reticulum unfolded protein response. *Nat Rev Mol Cell Biol* 2007; **8**: 519–529.
10. Wang XZ, Harding HP, Zhang Y, Jolicoeur EM, Kuroda M, Ron D. Cloning of mammalian Ire1 reveals diversity in the ER stress responses. *EMBO J* 1998; **17**: 5708–5717.
11. Wang Y, Shen J, Arenzana N, Tirasophon W, Kaufman RJ, Prywes R. Activation of ATF6 and an ATF6 DNA binding site by the endoplasmic reticulum stress response. *J Biol Chem* 2000; **275**: 27013–27020.
12. Harding HP, Zhang Y, Ron D. Protein translation and folding are coupled by an endoplasmic-reticulum-resident kinase. *Nature* 1999; **397**: 271–274.
13. Schroder M, Kaufman RJ. The mammalian unfolded protein response. *Annu Rev Biochem* 2005; **74**: 739–789.
14. Tabas I. Consequences of cellular cholesterol accumulation: basic concepts and physiological implications. *J Clin Invest* 2002; **110**: 905–911.
15. Zhang K, Kaufman RJ. Unfolding the toxicity of cholesterol. *Nat Cell Biol* 2003; **5**: 769–770.
16. Yao PM, Tabas I. Free cholesterol loading of macrophages induces apoptosis involving the fas pathway. *J Biol Chem* 2000; **275**: 23807–23813.
17. Yao PM, Tabas I. Free cholesterol loading of macrophages is associated with widespread mitochondrial dysfunction and activation of the mitochondrial apoptosis pathway. *J Biol Chem* 2001; **276**: 42468–42476.
18. Feng B, Yao PM, Li Y, Devlin CM, Zhang D, Harding HP *et al.* The endoplasmic reticulum is the site of cholesterol-induced cytotoxicity in macrophages. *Nat Cell Biol* 2003; **5**: 781–792.
19. Devries-Seimon T, Li Y, Yao PM, Stone E, Wang Y, Davis RJ *et al.* Cholesterol-induced macrophage apoptosis requires ER stress pathways and engagement of the type A scavenger receptor. *J Cell Biol* 2005; **171**: 61–73.
20. Aflaki E, Radovic B, Chandak PG, Kolb D, Eisenberg T, Ring J *et al.* Triacylglycerol accumulation activates the mitochondrial apoptosis pathway in macrophages. *J Biol Chem* 2011; **286**: 7418–7428.
21. Zimmermann R, Strauss JG, Haemmerle G, Schoiswohl G, Birner-Gruenberger R, Riederer M *et al.* Fat mobilization in adipose tissue is promoted by adipose triglyceride lipase. *Science* 2004; **306**: 1383–1386.
22. Jenkins CM, Mancuso DJ, Yan W, Sims HF, Gibson B, Gross RW. Identification, cloning, expression, and purification of three novel human calcium-independent phospholipase A2 family members possessing triacylglycerol lipase and acylglycerol transacylase activities. *J Biol Chem* 2004; **279**: 48968–48975.
23. Villena JA, Roy S, Sarkadi-Nagy E, Kim KH, Sul HS. Desnutrin, an adipocyte gene encoding a novel patatin domain-containing protein, is induced by fasting and glucocorticoids: ectopic expression of desnutrin increases triglyceride hydrolysis. *J Biol Chem* 2004; **279**: 47066–47075.

24. Chandak PG, Radovic B, Aflaki E, Kolb D, Buchebner M, Frohlich E *et al.* Efficient phagocytosis requires triacylglycerol hydrolysis by adipose triglyceride lipase. *J Biol Chem* 2010; **285**: 20192–20201.
25. Haemmerle G, Lass A, Zimmermann R, Gorkiewicz G, Meyer C, Rozman J *et al.* Defective lipolysis and altered energy metabolism in mice lacking adipose triglyceride lipase. *Science* 2006; **312**: 734–737.
26. Ma Y, Brewer JW, Diehl JA, Hendershot LM. Two distinct stress signaling pathways converge upon the CHOP promoter during the mammalian unfolded protein response. *J Mol Biol* 2002; **318**: 1351–1365.
27. Swanton C, Marani M, Pardo O, Warne PH, Kelly G, Sahai E *et al.* Regulators of mitotic arrest and ceramide metabolism are determinants of sensitivity to paclitaxel and other chemotherapeutic drugs. *Cancer Cell* 2007; **11**: 498–512.
28. Treiman M. Regulation of the endoplasmic reticulum calcium storage during the unfolded protein response–significance in tissue ischemia? *Trends Cardiovasc Med* 2002; **12**: 57–62.
29. Graier WF, Frieden M, Malli R. Mitochondria and Ca(2+) signaling: old guests, new functions. *Pflugers Arch* 2007; **455**: 375–396.
30. Amuthan G, Biswas G, Ananadatheerthavarada HK, Vijayasarathy C, Shephard HM, Avadhani NG. Mitochondrial stress-induced calcium signaling, phenotypic changes and invasive behavior in human lung carcinoma A549 cells. *Oncogene* 2002; **21**: 7839–7849.
31. Arnould T, Vankoningsloo S, Renard P, Houbion A, Ninane N, Demazy C *et al.* CREB activation induced by mitochondrial dysfunction is a new signaling pathway that impairs cell proliferation. *EMBO J* 2002; **21**: 53–63.
32. Timmins JM, Ozcan L, Seimon TA, Li G, Malagelada C, Backs J *et al.* Calcium/calmodulin-dependent protein kinase II links ER stress with Fas and mitochondrial apoptosis pathways. *J Clin Invest* 2009; **119**: 2925–2941.
33. Marciniak SJ, Yun CY, Oyadomari S, Novoa I, Zhang Y, Jungreis R *et al.* CHOP induces death by promoting protein synthesis and oxidation in the stressed endoplasmic reticulum. *Genes Dev* 2004; **18**: 3066–3077.
34. Nigam SK, Goldberg AL, Ho S, Rohde MF, Bush KT, Sherman M. A set of endoplasmic reticulum proteins possessing properties of molecular chaperones includes Ca(2+)-binding proteins and members of the thioredoxin superfamily. *J Biol Chem* 1994; **269**: 1744–1749.
35. Calfon M, Zeng H, Urano F, Till JH, Hubbard SR, Harding HP *et al.* IRE1 couples endoplasmic reticulum load to secretory capacity by processing the XBP-1 mRNA. *Nature* 2002; **415**: 92–96.
36. Orrenius S, Zhivotovsky B, Nicotera P. Regulation of cell death: the calcium-apoptosis link. *Nat Rev Mol Cell Biol* 2003; **4**: 552–565.
37. Tornquist K, Malm AM, Pasternack M, Kronqvist R, Bjorklund S, Tuominen R *et al.* Tumor necrosis factor-alpha, sphingomyelinase, and ceramide inhibit store-operated calcium entry in thyroid FRTL-5 cells. *J Biol Chem* 1999; **274**: 9370–9377.
38. Wong K, Li XB, Hunchuk N. N-acetylsphingosine (C2-ceramide) inhibited neutrophil superoxide formation and calcium influx. *J Biol Chem* 1995; **270**: 3056–3062.
39. Kroesen BJ, Pettus B, Luberto C, Busman M, Sietsma H, de Leij L *et al.* Induction of apoptosis through B-cell receptor cross-linking occurs via *de novo* generated C16-ceramide and involves mitochondria. *J Biol Chem* 2001; **276**: 13606–13614.
40. Schubert KM, Scheid MP, Duronio V. Ceramide inhibits protein kinase B/Akt by promoting dephosphorylation of serine 473. *J Biol Chem* 2000; **275**: 13330–13335.
41. Kitatani K, Idkowiak-Baldys J, Bielawski J, Taha TA, Jenkins RW, Senkal CE *et al.* Protein kinase C-induced activation of a ceramide/protein phosphatase 1 pathway leading to dephosphorylation of p38 MAPK. *J Biol Chem* 2006; **281**: 36793–36802.
42. Spiegel S, Milstien S. Sphingosine-1-phosphate: an enigmatic signalling lipid. *Nat Rev Mol Cell Biol* 2003; **4**: 397–407.
43. Basu SK, Goldstein JL, Anderson GW, Brown MS. Degradation of cationized low density lipoprotein and regulation of cholesterol metabolism in homozygous familial hypercholesterolemia fibroblasts. *Proc Natl Acad Sci USA* 1976; **73**: 3178–3182.

Supplementary Information accompanies the paper on Cell Death and Disease website (http://www.nature.com/cddis)